

Article

Adaptive-MPPT-Based Control of Improved Photovoltaic Virtual Synchronous Generators

Xiangwu Yan ^{1,*}, Jiajia Li ¹, Ling Wang ¹, Shuaishuai Zhao ¹, Tie Li ², Zhipeng Lv ³ and Ming Wu ³

¹ Key Laboratory of Distributed Energy Storage and Micro-Grid of Hebei Province, North China Electric Power University, Baoding 071003, China; lijiajia1018@163.com (J.L.); 13697662469@163.com (L.W.); zhao2017shuaishuai@163.com (S.Z.)

² State Grid Liaoning Electric Power Research Institute, Shenyang 110000, China; tony_fe@126.com

³ China Electric Power Research Institute (CEPRI), Beijing 100192, China; lvzhipeng@epri.sgcc.com.cn (Z.L.); wuming@epri.sgcc.com.cn (M.W.)

* Correspondence: xiangwuy@ncepu.edu.cn; Tel.: +86-139-0336-5326

Received: 15 June 2018; Accepted: 9 July 2018; Published: 12 July 2018



Abstract: The lack of inertia and damping mechanism of photovoltaic (PV) grid-connected systems controlled by maximum power point tracking (MPPT) poses a challenge for the safety and stability of the grid. Virtual synchronous generator (VSG) technology has attracted wide attention, since it can make PV grid-connected inverter present the external characteristics of a synchronous generator (SG). Nevertheless, traditional PV-VSG is generally equipped with an energy storage device, which leads to many problems, such as increased costs, space occupation, and post-maintenance. Thus, this paper proposes a two-stage improved PV-VSG control method based on an adaptive-MPPT algorithm. When PV power is adequate, the adaptive-MPPT allows the PV to change the operating point within a stable operation area to actualize system supply-demand, matching in accordance to the load or dispatching power demand; when PV power is insufficient, PV achieves traditional MPPT control to reduce power shortage; simultaneously, improved VSG control prevents the DC bus voltage from falling continuously to ensure its stability. The proposed control approach enables the two-stage PV-VSG to supply power to loads or connect to the grid without adding additional energy storage devices, the effectiveness of which in off-grid and grid-connected modes is demonstrated by typical simulation conditions.

Keywords: two-stage photovoltaic power; virtual synchronous generator; adaptive-MPPT (maximum power point tracking); improved-VSG (virtual synchronous generator); power matching

1. Introduction

In recent years, the continued consumption of fossil fuels has caused problems in terms of energy crises and environmental pollution [1]. One effective solution is exploiting and utilizing renewable energy sources, which play a crucial role in the transformation of the energy structure and are guided by the principle of sustainability [2]. Solar energy, due to the characteristics of green, clean, environmental friendliness and sustainability, enables photovoltaic (PV) power generation to be highly valued by countries all over the world [3,4]. Under the policy support of the ‘12th Five-Year Plan’ and ‘13th Five-Year Plan’ [4,5], the PV power market in China has enjoyed rapid development. In 2016, China became the country with the biggest PV power generation capacity in the world, with an accumulated installed capacity of 77.4 GW [3]. Furthermore, the ‘Notice on Matters Related to Photovoltaic Power Generation in 2018’ [6], issued by the National Development and Reform Commission, Ministry of Finance and National Energy Administration, further promotes the healthy and sustainable development of the PV industry, in which orderly development of distributed PV is

sustained, and PV poverty alleviation projects such as roof PVs [2] are supported. The above series of policies indicates that China's PV industry presents great potential for progress.

In the field of PV control technology, because early designers mainly consider economic benefits, PV systems usually adopt a maximum power point tracking (MPPT) control strategy for integration into the grid through a power electronic inverter [7,8]. However, the aforementioned control scheme belongs to passive control, which cannot actively respond to changes of grid frequency. In addition, PV systems do not possess dynamic characteristics consistent with conventional synchronous generators (SG), thanks to the deficiency of inverter inertia and damping [9–11], which is detrimental to improving the stability of frequency and voltage in the case of the grid interference, causing a potential threat to the security and stability of the power grid.

In July 2015, the 'Guidance on Promoting Smart Grid Development' [12] formulated by the National Energy Administration pointed out that "the grid-connected devices with plug-and-play and friendly grid-connected features will be promoted to meet the extensive access requirements of new energy and distributed generation". As a result, with the increasing of PV penetration, its grid-connected equipment needs to gradually alter the idea of "only power generation, regardless of power grid". Under the above background, ensuring high-proportional, large-scale PV power-friendly access from the "source" has become a major issue that needs to be resolved [13]. In view of the above-mentioned factors, some scholars have introduced virtual synchronous generator (VSG) technology [9,14] into the PV system due to its ability to make PV grid-connected inverters behave like SG. Indeed, VSG can offer inertia and damping to suppress rapid variations in voltage and frequency during the transient process; VSG-controlled PV systems autonomously participate in primary regulation to implement responsive interaction with the grid in the steady case.

In numerous studies [15–18], the DC side of the PV inverter is normally assumed to be a constant DC source, and the further investigation of VSG control is based on this foundation. This type of PV-VSG research ignores the potential impact of PV dynamic characteristics on VSG control, hence limiting the development of PV-VSG. For this reason, the cooperative operation mode of PV and energy storage is discussed in [19–22], which is referred to as a PV-storage system for short, in which the PV system adds a bidirectional energy storage device at the DC side to stabilize the DC bus voltage and realizes VSG function through the inverter. In the above PV-storage system, the output power of energy storage compensates for the deficiency of the PV dynamic characteristics and the variations of the load or dispatching requirements. However, in terms of VSG, the power involved in primary regulation derives from the energy storage instead of the PV power source. Moreover, the additional configuration of energy storage increases system cost and maintenance workload, as well as the additional installation space, making it difficult for practical application. Thus, with regard to this issue, a novel control strategy for a stand-alone PV system based on VSG which implements the combination of PV and VSG is proposed in [23], and this PV-VSG control scheme is extended to a grid-connected mode in [24]. The above-mentioned control mechanism eliminates the energy storage configuration of PV-VSG, and takes the PV power source as a virtual prime mover of the virtual synchronous generator, which balances system power according to the actual power demands. Nevertheless, the above PV-VSG control structure is only applied to the centralized PV inverter with single-stage DC/AC topology, which is inappropriate for a string PV inverter with two-stage DC/DC and DC/AC circuits where the networking is flexible and the MPPT voltage adjustment range is wider.

Drawing on the control concept of the single-stage PV-VSG, it is hoped that the two-stage PV-VSG could minimize the energy storage allocation, the realization of which faces two difficulties: First, it is difficult to actualize the combination of PV with VSG, since it has complex dynamic features, operational stability requirements and limited capacity. Next, compared with a single-stage system, the DC bus voltage is no longer the PV voltage, the regulation of which would be more complicated. To deal with these two problems, we can draw lessons from how the wind farm modifies the power tracking curve to achieve the supply-demand matching [25–27]. Under the premise of not adding energy storage, taking the power-voltage output characteristic of PV as a research point, the output power of PV arrays

is regulated by a DC/DC converter, which can be directly interfaced with local loads or power grids through post-stage VSG.

On the basis of the analysis above, considering the volatility and finiteness of PV, in this paper, a two-stage improved PV-VSG control approach founded on an adaptive-MPPT algorithm is proposed. When PV power is sufficient, adaptive-MPPT enables the PV system to send power identical to the load or dispatching power requirements, which does not export maximum power all the time; in the case of PV power deficiency, the adaptive-MPPT algorithm turns into traditional MPPT control; meanwhile, improved-VSG heightens the DC bus voltage stability. This control approach obviates the energy storage configuration of the traditional two-stage PV-VSG, thereby reducing investment and maintenance costs. An adaptively regulated two-stage PV-VSG system is established in MATLAB, and the effective combination of the two-stage PV and VSG is verified through simulation in off-grid and grid-connected modes, respectively. In off-grid mode, the novel two-stage PV-VSG sends power in accordance with the load demand and provides voltage and frequency support for load; in grid-connected mode, AC voltage and frequency are sustained by the power grid, and PV-VSG is responsible for delivering power following the dispatching instruction.

2. Overview of Fundamental Problems

The typical PV micro-grid system, which is composed of photovoltaic generation, energy storage device and diesel generator, supplies the local loads or accesses the grid, as illustrated in Figure 1. For ease of reading, the PV system is marked with a red frame in Figure 1.

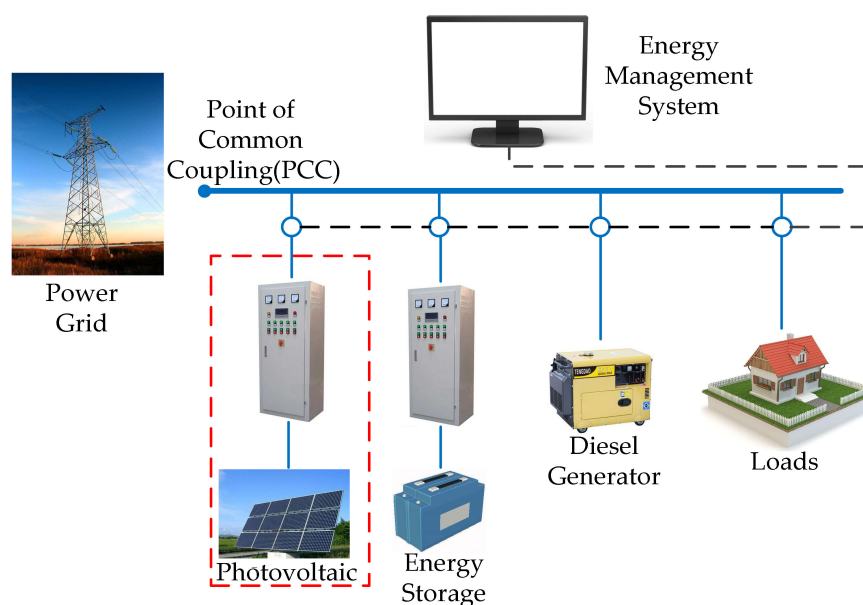


Figure 1. The photovoltaic (PV) micro-grid system.

Picking up the PV system in the above typical PV micro-grid as an important research target, it is desirable for the PV system to achieve friendly access through the application of VSG technology. In a general way, in related works [19,20], a PV-VSG control strategy installed with an energy storage battery on the DC side was adopted, as shown in Figure 2. For traditional PV-VSG control, since PV output power is particularly influenced by environmental factors such as light intensity and temperature [13], the energy storage battery is primarily responsible for balancing power through a DC/DC converter so as to match the required power. However, the above control exhibits two defects: the implementation of the VSG function is overly dependent on the energy storage battery, so the inverter may not continue to work once the energy storage battery failure occurs. Secondly, the energy storage configuration of PV-VSG will greatly increase the expenses of investment, operation and maintenance [23,28].

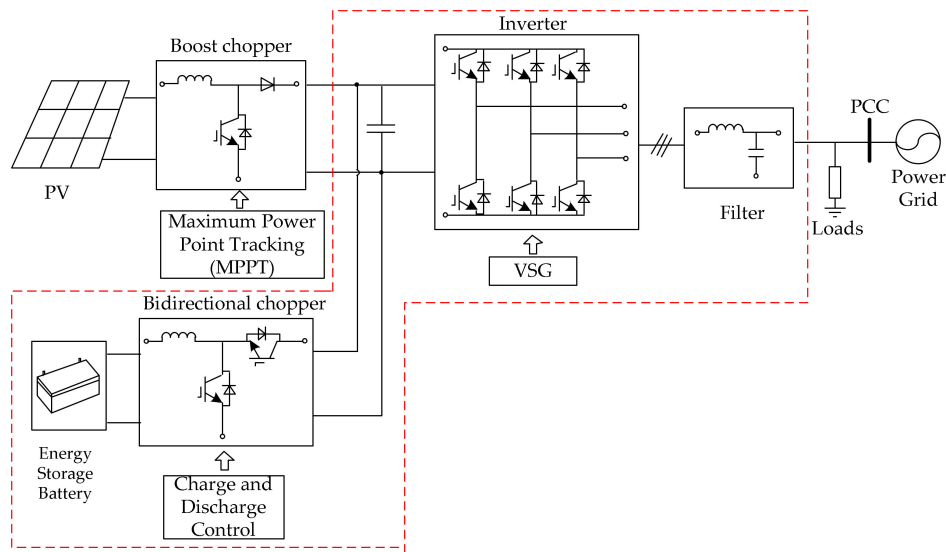


Figure 2. The traditional PV-VSG (photovoltaic-virtual synchronous generator) control oriented for the energy storage battery [19,20].

In order to resolve the inherent problems in Figure 2, a novel two-stage PV-VSG control approach is advanced in Figure 3, which consists of an adaptive-MPPT control and an improved-VSG control. Although the energy storage battery of PV-VSG is removed, the joint control of the adaptive-MPPT and improved-VSG still stabilizes the DC bus voltage and achieves power matching.

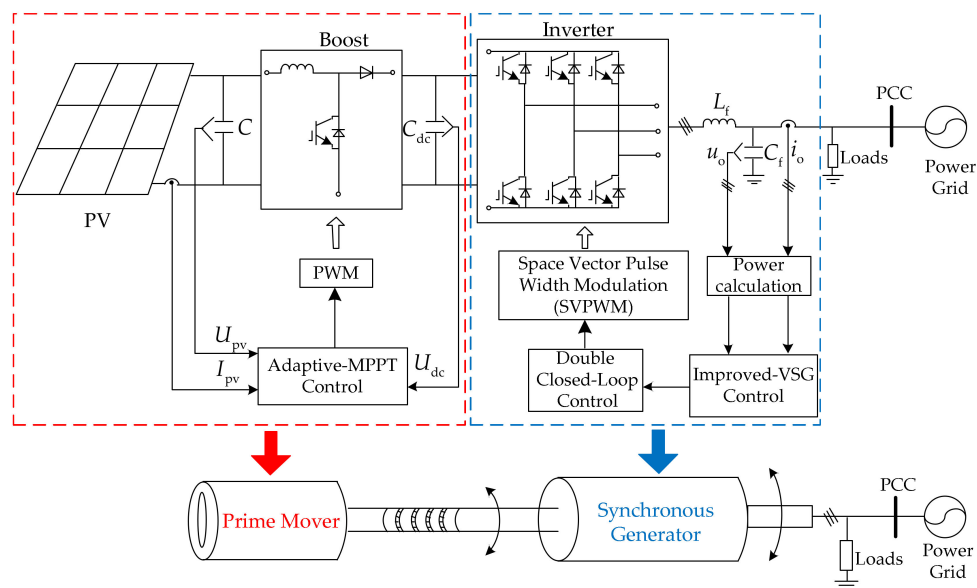


Figure 3. The main circuit topology and control method of the presented two-stage PV-VSG.

As is evident from Figure 3, the pre-stage PV-Boost circuit comprises a prime mover using adaptive-MPPT control, and the post-stage inverter controlled by improved-VSG forms a synchronous generator. In this way, employing the prime mover as a power source drives the synchronous generator to send power to the loads or the power grid. Evidently, unlike the traditional PV-VSG with an energy storage battery as the prime mover in Figure 2, this novel control approach can solve the power balance problem of two-stage PV-VSG from the source and economizes various costs associated with configuring energy storage.

In general, the proposed two-stage PV-VSG possesses two operational scenarios:

- (1) PV maximum available power is adequate.

When PV maximum output power is greater than the power required by the load or dispatch instruction, operational power depends on load or dispatching requirements, and the major challenge is guaranteeing system power balance. At this moment, PV controlled by adaptive-MPPT changes the operating point to decrease power output according to load or dispatching power demand, which ensures supply-demand matching.

- (2) PV maximum available power is inadequate.

The insufficiency of the PV maximum available power signifies that the maximum output of PV is less than the load or dispatching demand power. Under this scenario, the major challenge is to control PV to provide as much power as possible and to ensure the overall stability of the PV-VSG system. Thus, adaptive-MPPT-controlled PV should operate at the maximum power point (MPP), which exports maximal power to minimize power shortage. Meanwhile, improved-VSG control prevents the DC bus voltage from dropping down continuously, so as to warrant the stability of the DC bus voltage.

Most notably, for the PV system, when the PV maximum available power is inadequate (the operation scenario (2)), if the load or dispatching power demands are still necessary to satisfy, other power supplies, such as energy storage and diesel generators in typical PV micro-grids (as shown in Figure 1), ought to offer power to compensate for the power shortage. This paper mainly aims at the operation scenarios of a single two-stage PV-VSG system and addresses problems of immediately accessing two-stage PV power by way of VSG without supernumerary energy storage devices; consequently, coordination control of the other power supplies and PV systems is no longer necessary to describe.

3. Methods

With regard to the two-stage PV system made up of PV-Boost circuit and inverter, control strategies include pre-stage adaptive-MPPT and post-stage improved-VSG, which are analyzed in detail in the subsequent subsections.

3.1. PV-Boost Control

3.1.1. Overall Control Scheme of Pre-Stage PV-Boost

Figure 4 displays the complete control scheme of the pre-stage PV-Boost. Since the research emphasis of this section is the pre-stage control, the post-stage inverter circuit is omitted, and is discussed in Section 3.2. The PV voltage reference U_{pv-ref} , which is obtained through the adaptive-MPPT control, and the actual value U_{pv} generate the PWM modulated signals D through PI control. The theoretical analysis of adaptive-MPPT algorithm will be elaborated in Section 3.1.2.

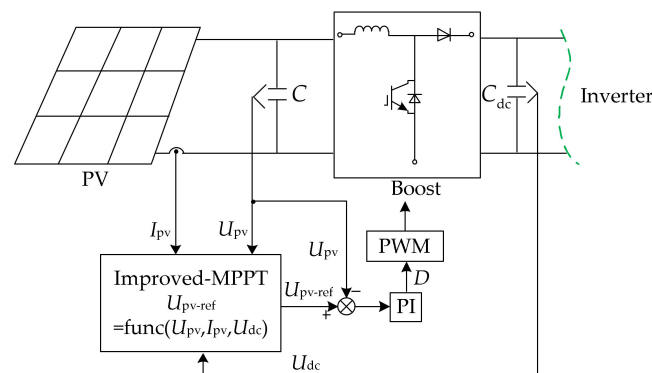


Figure 4. Overview of control scheme for pre-stage PV-Boost.

3.1.2. Adaptive-MPPT Algorithm

Regarding the PV power-voltage (P - U) characteristic curve [28–30] (as shown in Figure 5) as a research core point, and taking advantage of regulating function of DC/DC converter on output power of PV cells, the adaptive-MPPT adjusts the working point in the stable operation area to fulfill supply-demand matching on the basis of actual power demands. From Figure 5, abscissa U_{pv} and ordinate P_{pv} represent the PV output voltage and output power, respectively. P_{max} is the PV maximum output power, which corresponds to the voltage U_{mpp} . Additionally, A , B and M are possible PV operating points, where M is the maximum power point.

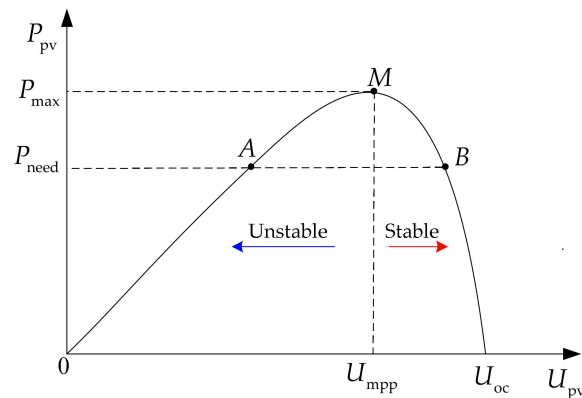


Figure 5. PV Power-voltage (P - U) characteristic curve.

Figure 5 shows that the PV operation area is divided into two regions based on the M point. When external power demand P_{need} is less than the PV maximum available power P_{max} , PV exists at two operating points: A and B . Through quantitative and qualitative verification, Refs. [23,24] indicate that the PV stable operation area is $[U_{mpp}, U_{oc}]$. Thus, combined with the actual operating conditions, the adaptive-MPPT should be equipped with the dynamic regulation features as follows:

- When $P_{need} < P_{max}$, PV works at B point within $[U_{mpp}, U_{oc}]$ to output power equal to P_{need} .
- When $P_{need} \geq P_{max}$, PV works at M point to output maximum power P_{max} .

Accordingly, taking into account the DC bus voltage U_{dc} , this paper designs the adaptive-MPPT algorithm based on an improved incremental conductance method in light of the following four control goals, as described in Figure 6.

- (1) Ensure that PV operates within the stable operating area $[U_{mpp}, U_{oc}]$.
- (2) Whether the DC bus voltage U_{dc} is stable at the set reference value U_{dc-ref} is used as a criterion for judging whether supply and demand match.
- (3) When the PV output power is in surplus, adaptive-MPPT causes the DC bus voltage to remain at the set reference value U_{dc-ref} constantly.
- (4) When the PV maximum output is insufficient at a given time, $U_{dc} < U_{dc-ref}$, adaptive-MPPT runs MPP to determine maintain maximum output.

From Figure 6, λ is a fixed step, and this adaptive-MPPT algorithm runs as follows:

- (1) When the PV system starts for the first time, the slope is $dI_{pv}/dU_{pv} + I_{pv}/U_{pv} > 0$. To prevent PV from operating in unstable areas, the algorithm enables PV run to $[U_{mpp}, U_{oc}]$ with $y = 1$, which ensures accurate tracking in the stable region all the time.
- (2) In the stable area, according to difference-value ΔU_{dc} sign of the actual DC bus voltage U_{dc} and set value U_{dc-ref} , PV regulates output power to meet supply-demand matching, i.e., $P_{pv} = P_{need}$. There are three main situations.

- When $\Delta U_{dc}(k) > 0$, in this case, $P_{pv}(k) > P_{need}(k)$, the PV output power should be reduced, so the voltage judgement sign is $x = -1$.
- When $\Delta U_{dc}(k) < 0$, in this case, $P_{pv}(k) < P_{need}(k)$, the PV output power ought to increase, so the voltage judgement sign is $x = 1$.
- When $\Delta U_{dc}(k) = 0$, in this case, $P_{pv}(k) = P_{need}(k)$, the voltage judgement sign is $x = 0$.

Nevertheless, since the actual adjustment direction is opposite to the voltage judgment sign in the stable area, the PV regulates with $y = -x$. Most notably, If the PV maximum output power is less than the load or the dispatch demand invariably, ΔU_{dc} is always less than zero, so $y = -x = -1$. Thus, this algorithm jumps out of the ΔU_{dc} judgment step and turns into the traditional MPPT control based on the conductance increment method.

- (3) The actual step size $y \times \lambda$ is obtained, thereby refreshing the PV voltage value U_{pv} .

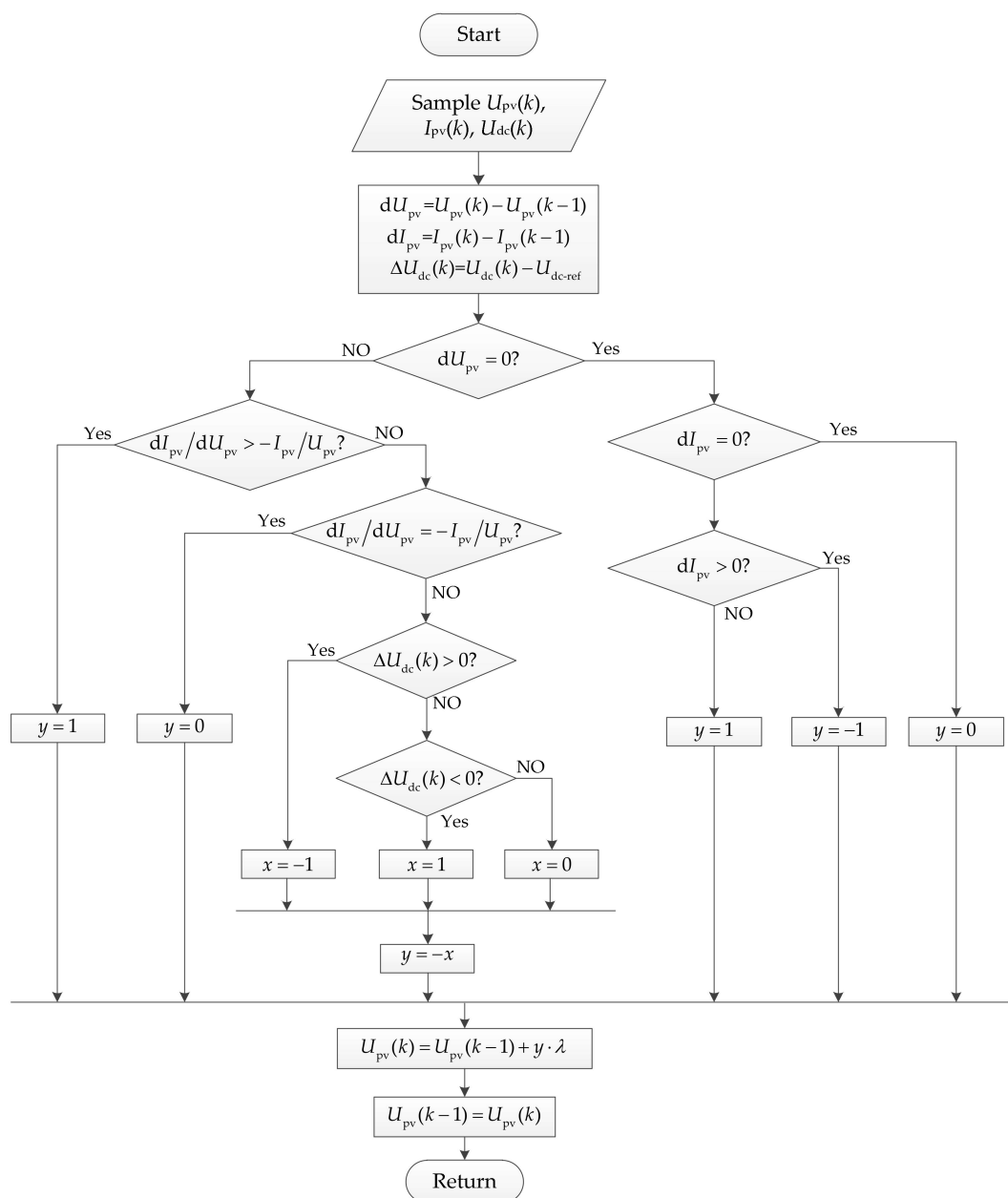


Figure 6. Adaptive-MPPT algorithm.

In conclusion, compared to traditional MPPT control, which always outputs maximum power [29,30], the proposed adaptive-MPPT algorithm, which is applied to the pre-stage PV-DC/DC circuit, possesses two contributions:

- In the case of sufficient PV power, adaptive-MPPT enables two-stage PV to transmit power in accordance with the load or dispatching requirements, while guaranteeing DC bus voltage $U_{dc} = U_{dc-ref}$.
- Under conditions where PV maximum output power is inadequate, adaptive-MPPT automatically switches to traditional MPPT control, always outputting maximum power to decrease the power shortage. At this moment, the DC bus voltage is no longer controlled.

3.2. Inverter Control

3.2.1. VSG Basic Modeling

The classical second-order model of synchronous generator (SG) is introduced into the VSG control to emulate the inertia and damping characteristics [31,32], including the rotor motion equation and the stator voltage equation, as expressed in Equations (1) and (2). In addition, droop control is used for mimicking the frequency regulator and excitation controller of SG, as shown in Equation (3).

$$J \frac{d\omega}{dt} = \frac{P_m - P_e}{\omega} - D(\omega - \omega_g) \tag{1}$$

$$e_{abc} = u_{abc} + Ri_{abc} + L \frac{di_{abc}}{dt} \tag{2}$$

where P_m is the mechanical power; P_e is the electromagnetic power; J and D represent the inertia and damping, respectively; ω is the rotor angular frequency; ω_g is the actual angular frequency of the grid; e_{abc} , u_{abc} and i_{abc} are the excitation voltage, terminal voltage and stator current of SG respectively, which correspond to input voltage, output voltage and output current in the inverter; R is the armature resistance and L is the synchronous reactance.

$$\begin{cases} U = U_N + D_p(P_N - P) \\ \omega_g = \omega_N + D_q(Q_N - Q) \end{cases} \tag{3}$$

where P_N and Q_N are the rated active power and reactive power, respectively; P and Q are the active power and reactive power of VSG; D_p is the P - ω droop coefficient and D_q is the Q - U droop coefficient; U_N is the rated voltage amplitude; ω_N is the rated angular frequency.

The combination of the classical second-order model and droop control constitutes the VSG basic model, whose control structure is depicted in Figure 7. VSG output power simulates the electromagnetic power, i.e., $P = P_e$.

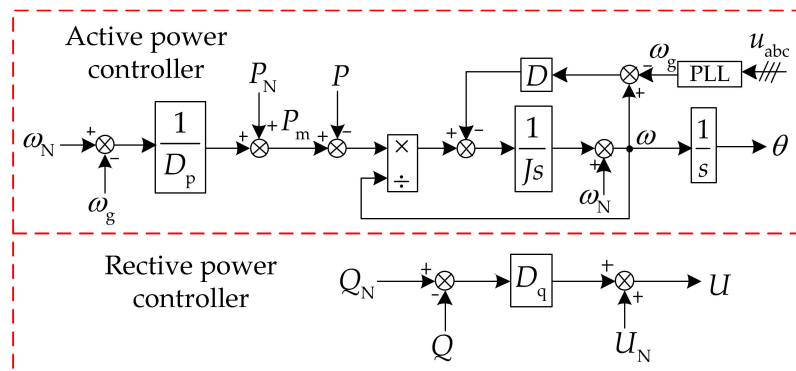


Figure 7. Basic control for VSG.

3.2.2. Improved-VSG Control

When the load or grid demands exceed the PV maximum available power, in order to diminish the power shortage, the DC bus capacitor C_{dc} will discharge. If this power shortage is larger, the DC bus voltage may constantly drop or even collapse, which endangers the stability of the system. To settle this problem, Figure 8 puts forward the improved-VSG control method which comprises of VSG basic control and additional control.

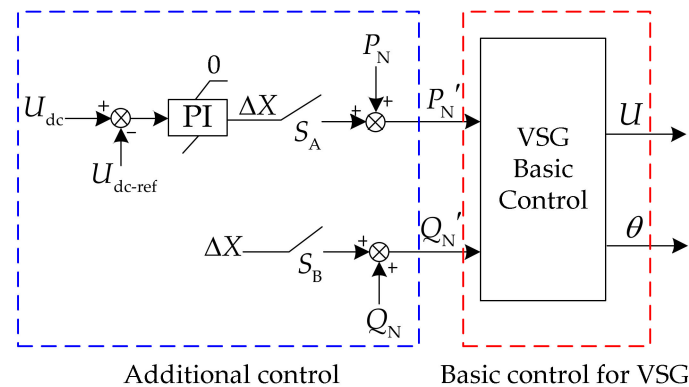


Figure 8. Improved-VSG control.

From Figure 8, the VSG basic control enables the PV inverter to take on the same inertia, damping and primary regulation characteristics as the SG, and the additional control is in charge of avoiding the DC bus voltage from falling continuously to ensure stability. For additional control, the difference between the measured DC bus voltage U_{dc} and the set-point U_{dc-ref} is regulated by PI control to obtain an additional control variable ΔX ; moreover, $\Delta X \leq 0$. The working mode of the additional control is as below:

- In off-grid mode, switch S_B is closed, while switch S_A is open, so ΔX is introduced into the reactive power loop to revise the reactive power reference Q_N' , i.e., $Q_N' = Q_N + \Delta X \leq Q_N$.
- In grid-connected mode, switch S_A is closed. Since voltage is sustained by the bulk power system, switch S_B is open. Active power reference P_N' is modified by ΔX , i.e., $P_N' = P_N + \Delta X \leq P_N$.

The basic principles of additional control are given by the following two aspects:

- (1) When the PV output power is surplus, pre-stage adaptive-MPPT changes the working point to achieve $P_{pv} = P_{need}$, so that the DC bus voltage can stabilize at the reference value U_{dc-ref} . Thus, $\Delta X = 0$, the additional control is inoperative, in this case, the adaptive-MPPT cooperates with VSG basic control.
- (2) When the PV maximum output is insufficient, i.e., $P_{max} < P_{need}$, although MPPT keeps PV outputting maximum power at all times, it still cannot meet the load or dispatch power requirements. Consequently, the DC bus capacitance will discharge, with the result that U_{dc} failed to keep at U_{dc-ref} . If the power difference-value is higher, U_{dc} will continue to fall until it collapses. In such situations, additional control takes effect.

- In off-grid mode, load power is related to voltage. ΔX acts on the reactive power loop to indirectly decrease the voltage amplitude, so as to reduce the inverter output power, which lowers the decline degree of U_{dc} to improve the PV steadiness.
- In grid-connected mode, the dispatching power is greater than the PV maximum output, resulting in insufficient power. ΔX is led into the active power loop to lessen dispatching power reference value, which prevents U_{dc} from falling ceaselessly.

Even if the DC bus voltage U_{dc} is jointly controlled by the pre-stage adaptive-MPPT and the post-stage improved-VSG, the two stages of control do not affect each other. When $P_{pv} > P_{need}$, the pre-stage U_{dc} plays a role, but the post-stage U_{dc} does not perform due to $\Delta X = 0$; when $P_{pv} < P_{need}$, the adaptive-MPPT changes into the traditional MPPT, in which U_{dc} is not governed. At this point, the post-stage U_{dc} is under control on account of $\Delta X < 0$.

To prove the effectiveness, we compared improved-VSG control with VSG basic control through simulation in off-grid and grid-connected mode. Before 1 s, $P_{max} > P_{need}$, and after 1 s, $P_{max} < P_{need}$. The simulation results are shown in Figure 9, in which the blue line represents the improved-VSG control and the red line is the VSG basic control.

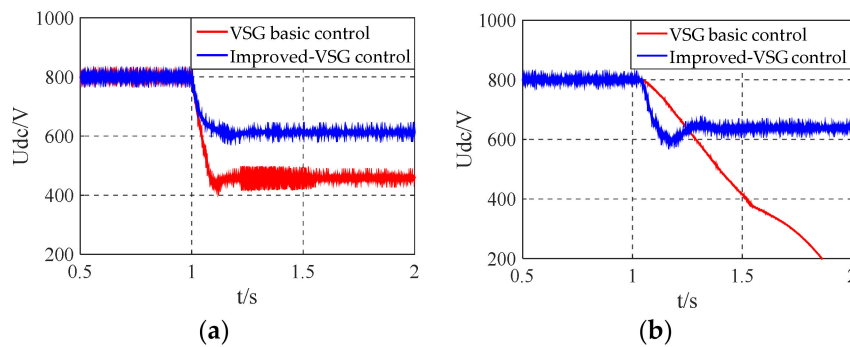


Figure 9. Comparison of DC bus voltage U_{dc} (a) Off-grid mode; (b) Grid-connected mode.

Apparently, as can be observed from the red line in Figure 9, when $P_{max} < P_{need}$, U_{dc} with VSG, basic control drops considerably whether in off-grid mode or grid-connected mode. Especially in the grid-connected mode, this case is more serious. However, when adopting the improved-VSG control, although PV maximum output cannot meet the power demand, it is manifestly known from the blue line in Figure 9 that the improved-VSG control can forestall incessant falling of U_{dc} and drastically reduce the U_{dc} drop degree to guarantee PV system stability. Therefore, later simulation validation will make use of the proposed improved-VSG control.

In summary, the improved-VSG that governs the post-stage inverter is provided with following properties:

- In situations of adequate PV power, the adaptive-MPPT-controlled pre-stage DC/DC converter accomplishes stability of the DC bus voltage, which can be considered a constant DC source. At this point, post-stage improved-VSG control mainly causes the inverter to present inertia, damping and primary regulation characteristics of the SG, that is, achieving VSG basic function.
- When the PV power is inadequate, the DC bus voltage is not managed by pre-stage DC/DC circuit anymore, since adaptive-MPPT changes into a traditional MPPT. Under this condition, additional control of the improved-VSG is effective to prevent the continuous drop of the DC bus voltage, thus enhancing the stability of the PV system.

3.2.3. Complete Control Scheme of Post-Stage Inverter

For the studied case, an overview of the applied control scheme for the post-stage inverter is displayed in Figure 10. The DC-side capacitor C_{dc} should be attached to the PV-Boost circuit, whose control method is discussed in Figure 4.

The control structure of the inverter has two layers of cascaded controllers, including the power controller, which is comprised of improved-VSG control, and a double closed-loop controller, which is formed of voltage outer-loop control and current inner-loop control. The outer-layer power controller basically emulates the main characteristic of the SG, and ensures the stability of the DC bus voltage when the PV power is inadequate. The inner-layer double closed-loop controller availably enhances the wave

quality of the inverter output. Afterwards, the inner-loop current control provides the modulation index for SVPWM which generates the pulse signals of the inverter switching transistor.

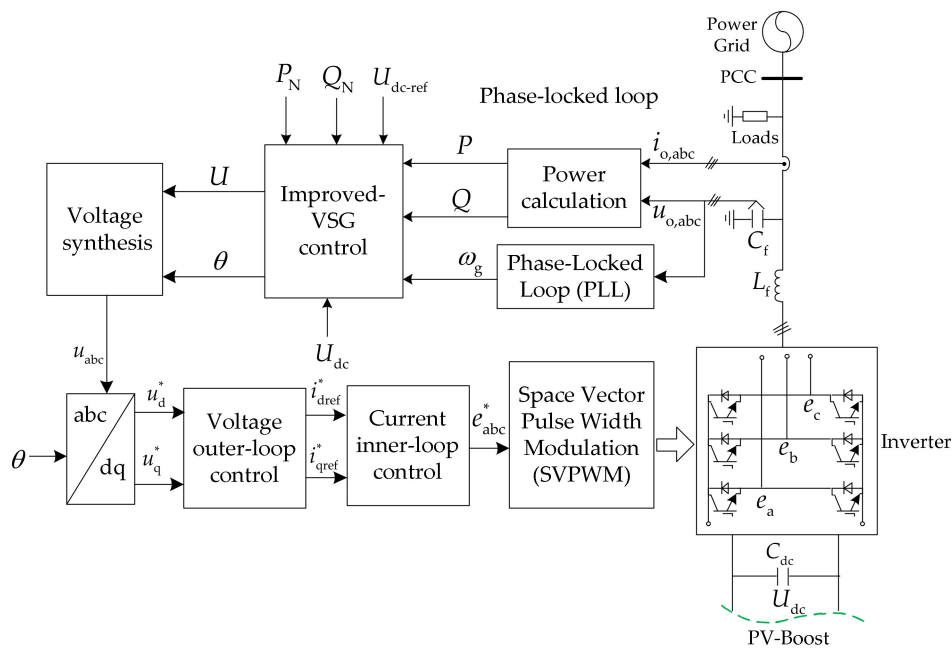


Figure 10. Complete control scheme of post-stage inverter.

4. Results

4.1. Simulation System and Simulation Parameters

The integrated system model of a single two-stage PV-VSG connected to the loads or power grid is built on the MATLAB/Simulink, as shown in Figure 11. Under the off-grid/grid-connected mode, the performance of the proposed control is validated.

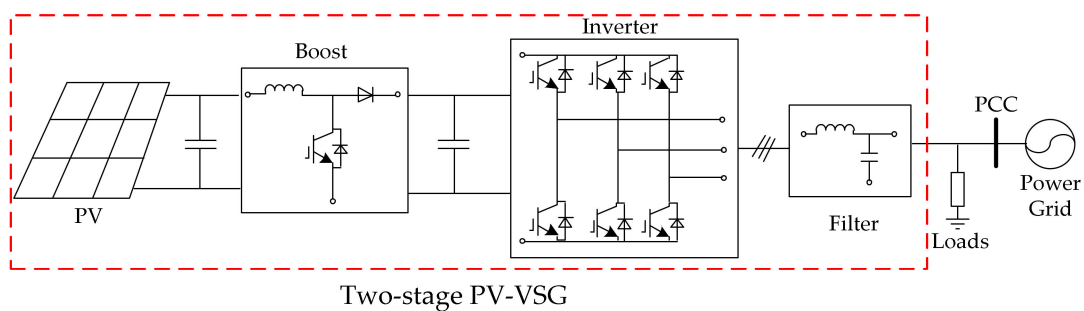


Figure 11. Schematic diagram of a single two-stage PV-VSG connects to the loads/power grid.

The photovoltaic cell type is First Solar FS-380. The DC/DC converter is a Boost circuit, which is controlled by the adaptive-MPPT in Section 3.1. The DC/AC inverter adapts the improved-VSG control presented in Section 3.2.

The main component parameters of the investigated system are reported in Table 1.

Table 1. Simulation parameters.

	Parameters	Values
Boost circuit parameters	PV-side capacitance, C	30 μ F
	Inductance, L	1 mH
	DC side capacitance, C_{dc}	5000 μ F
Filter parameters	The series inductance of the filter, L_f	10 mH
	The parallel capacitance of the filter, C_f	350 μ F
System parameters	Reference value of DC voltage, U_{dc-ref}	800 V
	Rated frequency	50 Hz
	The rated phase voltage of power system	220 V
	Inverter switching frequency	5 kHz
Control parameters	The P - ω droop coefficient, D_p	0.0003
	The Q - U droop coefficient, D_q	0.003
	The virtual inertia of VSG, J	0.1
	The virtual damping of VSG, D	20
	The proportionality factor of additional control in improved-VSG control, P_{Udc}	50
	The integration factor of additional control in improved-VSG control, I_{Udc}	0.01

4.2. Verification Process

For the typical PV microgrid system shown in Figure 1, there are two operating ways: off-grid mode and grid-connected mode. Focusing on the PV system in the above microgrid, we attest the effectiveness that pre-stage PV power implements direct access through post-stage VSG in the absence of allocating energy storage device. Thus, taking the single two-stage PV system in Figure 11 as an example, the variations of the load or scheduling demand power and PV maximum output are respectively set up to verify the proposed control method.

4.2.1. Off-Grid Mode

Under the off-grid mode, since this paper only simulates a single PV system, the inverter output voltage will decrease due to the power shortage when PV maximum power is not enough. In this case, the power shortage should be supplemented by other power sources of the PV microgrid in Figure 1, such as an energy storage battery or diesel generator, to ensure power quality, which is not the research emphasis in this paper, so the coordination control of the other power sources and PV system is omitted. This part is also outlined in Section 2 (2).

When the system works in off-grid mode, the two-stage PV-VSG which supplies to the loads provides the frequency and voltage support for the loads.

(1) Variation of Load Demand

The external environment remains constant. PV maximum available power is $P_{max} = 15$ kW and the corresponding output voltage is $U_{mpp} = 370$ V. Before 1 s, the power demand of the load is 12 kW, which is reduced to 10 kW at 1 s but increased to 18 kW at 1.5 s. Figure 12 displays the system dynamic response waveforms in the case of varying load requirements.

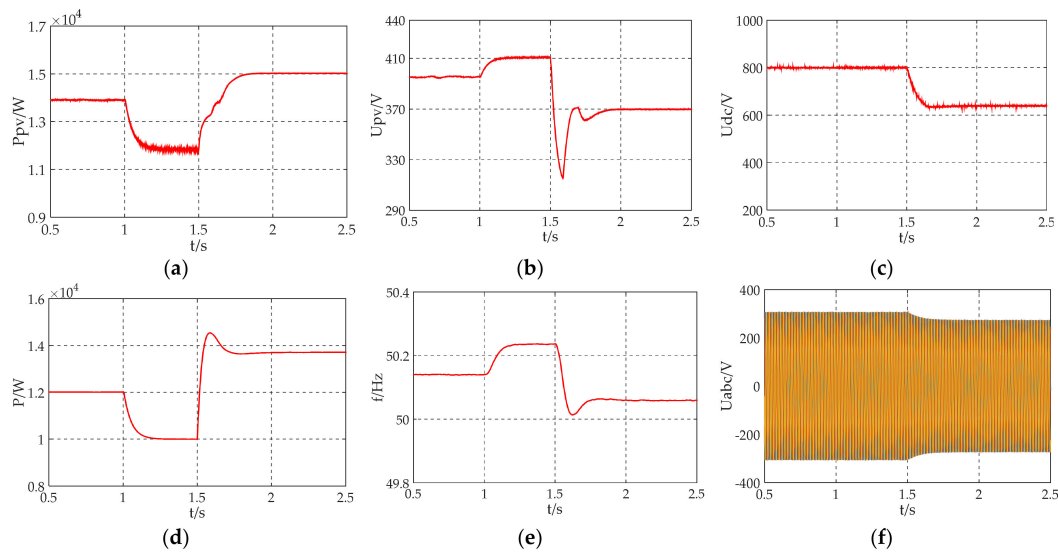


Figure 12. Waveforms in the off-grid mode when load demand changes (a) PV output power; (b) PV output voltage; (c) DC bus voltage; (d) Inverter output power; (e) VSG frequency; (f) Inverter output voltage.

Before 1 s and between 1~1.5 s, the load demand power is 12 kW and 10 kW, respectively, which is less than PV maximum output power 15 kW, i.e., $P_{\max} > P_{\text{need}}$, so the PV power is surplus. Thus, it can be seen in Figure 12a,d that PV power controlled by adaptive-MPPT changes the operating point to make inverter output power match the load demand. Additionally, before 1.5 s, Figure 12b shows that PV output voltage is greater than $U_{\text{mpp}} = 370$ V, i.e., $U_{\text{pv}} > U_{\text{mpp}}$, which means that PV works in the stable area $[U_{\text{mpp}}, U_{\text{oc}}]$. Furthermore, DC bus voltage stabilizes at the set value 800 V owing to system power balance in Figure 12c, and inverter output voltage is identical to the AC rated voltage in Figure 12f. After 1.5 s, the load demand power increases to 18 kW, which is greater than the PV maximum output power of 15 kW, i.e., $P_{\max} < P_{\text{need}}$; as a result, the PV power is inadequate. In this case, Figure 12a,b indicates that PV works at MPP point (370 V, 15 kW) to output maximum power. In addition, due to power shortage, the DC bus voltage reduces to 625 V in Figure 12c and the inverter output voltage falls below the rated AC voltage in Figure 12f. During the above power regulation process, Figure 12e shows that VSG frequency is involved in regulating according to the active droop coefficient.

(2) Variation of PV Maximum Output Power

The load demand power remains at 10 kW continuously. The variation of the PV maximum output power is emulated by changing light intensity, whose parameter settings are shown in Table 2. Figure 13 shows the simulation waveforms when changing PV maximum output power.

Table 2. Light intensity parameters.

Time (s)	Light Intensity (W/m ²)	P_{\max} (kW)	U_{mpp} (V)
Before 1 s	1000	15	370
1~1.5 s	1200	18.2	380
After 1.5 s	700	9.5	342

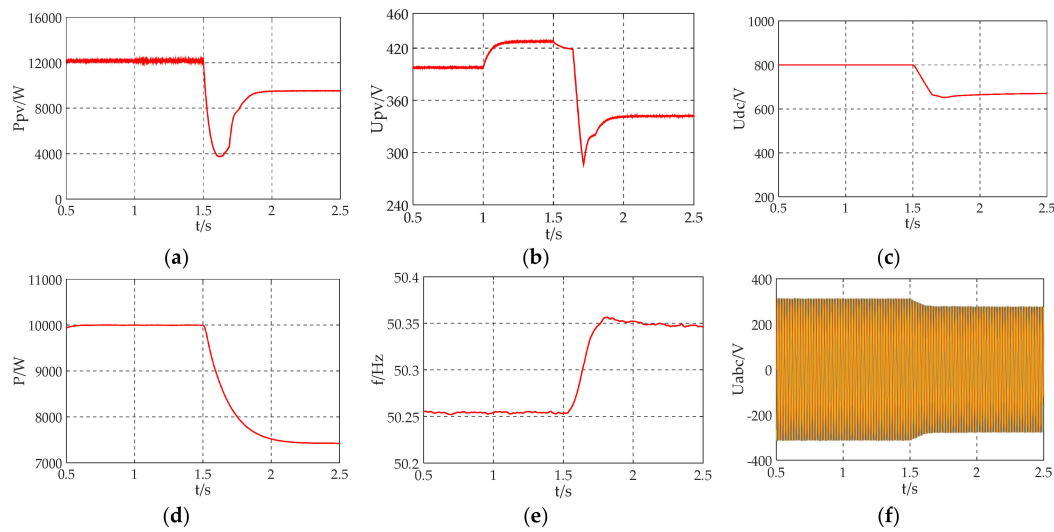


Figure 13. Waveforms in the off-grid mode when PV maximum output power changes (a) PV output power; (b) PV output voltage; (c) DC bus voltage; (d) Inverter output power; (e) VSG frequency; (f) Inverter output voltage.

Before 1 s and between 1~1.5 s, Table 2 illustrates that the PV maximum power is 15 kW and 18.2 kW, respectively, which are greater than the load demand power 10 kW, i.e., $P_{\max} > P_{\text{need}}$. Figure 13a,d demonstrates that the PV power decreases the output power to enable inverter output of 10 kW power, which is equal to the load requirement. Despite the increased light intensity, the PV output remains unchanged due to the constant load demand in Figure 13a. We can see from Figure 13b that PV output voltage is 398 V before 1 s and 428 V between 1~1.5 s, which are more than 370 V and 380 V, respectively, so the PV power based on the adaptive-MPPT algorithm adjusts the working point in the stable region $[U_{\text{mpp}}, U_{\text{oc}}]$. The VSG frequency in Figure 13e also stays constant on account of power demand invariability. Due to supply-demand matching before 1.5 s, the DC bus voltage can hold at 800 V in Figure 13c and the amplitude of the inverter output voltage is 311.13 V. After 1.5 s, $P_{\max} < P_{\text{need}}$, it can be seen from Figure 13a,b that PV power runs at the MPP point (9.5 kW, 342 V), which proves that adaptive-MPPT can be transformed into a traditional MPPT control when PV maximum is inadequate. VSG frequency regulation in Figure 13e depends on the droop characteristic. Figure 13c shows that the improved-VSG let the DC bus voltage stabilize at 670 V. Due to the existence of power shortage, the inverter output voltage is below the rated amplitude 311.13 V.

4.2.2. Grid-Connected Mode

In grid-connected mode, the AC voltage is backed by the bulk power grid, and the VSG is mainly aimed at contenting the dispatching power demand.

(1) Variation of Dispatching Power Demand

During the simulation process, the external environment is configured on be fixed, that is, the PV maximum available power is $P_{\max} = 15$ kW, which corresponds to output voltage $U_{\text{mpp}} = 370$ V. Before 1 s, the dispatching power instruction was 11 kW, which decreased to 9 kW at 1 s and increased to 16 kW at 1.5 s. In this case, the simulation results are expressed in Figure 14.

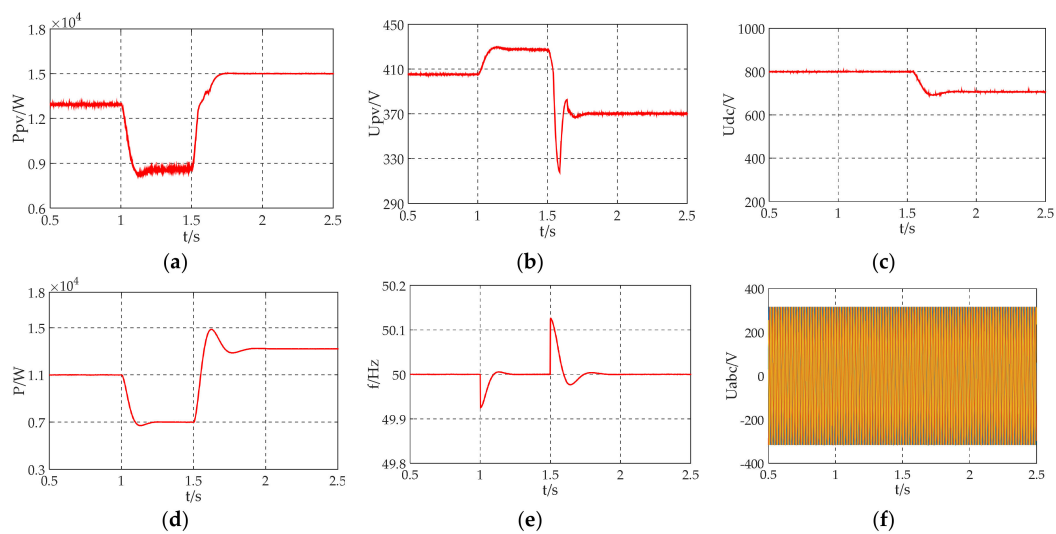


Figure 14. Waveforms in the grid-connected mode when dispatching power demand changes (a) PV output power; (b) PV output voltage; (c) DC bus voltage; (d) Inverter output power; (e) VSG frequency; (f) Inverter output voltage.

Before 1 s and between 1~1.5 s, the PV maximum available power 15 kW exceeded the dispatching demand power of 11 kW and 9 kW, i.e., $P_{\max} > P_{\text{need}}$. Thus, can be observed in Figure 14a,b,d that PV adaptively regulates in the stable interval ($U_{\text{pv}} > 370$ V), so that the inverter outputs power of 11 kW and 7 kW, which are identical to the dispatch orders. On account of system power balance, the DC bus voltage maintains at 800 V in Figure 14c. After 1.5 s, the dispatching requirements surpass the PV maximum power, i.e., $P_{\max} = 15$ kW $<$ $P_{\text{need}} = 16$ kW. At this time, PV power operates at the MPP point (15 kW, 370 V) to achieve full output. Moreover, improved-VSG causes the DC bus voltage to settle at 710 V, so as to ensure its stability. Throughout the adjustment process, because of the rigid support offered by the bulk power grid, the VSG frequency in Figure 14e maintains at the rated value of 50 Hz after slight fluctuations, and the inverter output voltage in Figure 14f is the same as the AC voltage of the bulk power grid.

(2) Variation of PV Maximum Output Power

The dispatch power demand is consistently 12 kW. The simulation conditions are in agreement with the variation of PV maximum output power under the off-grid model. The light intensity is 1000 W/m² before 1 s, but it rises to 1200 W/m² at 1 s and then weakens to 700 W/m² at 1.5 s. Other relevant PV parameters of the PV power and voltage are indicated in Table 2. Figure 15 gives the simulation waveforms in grid-connected mode when the PV maximum output power changes.

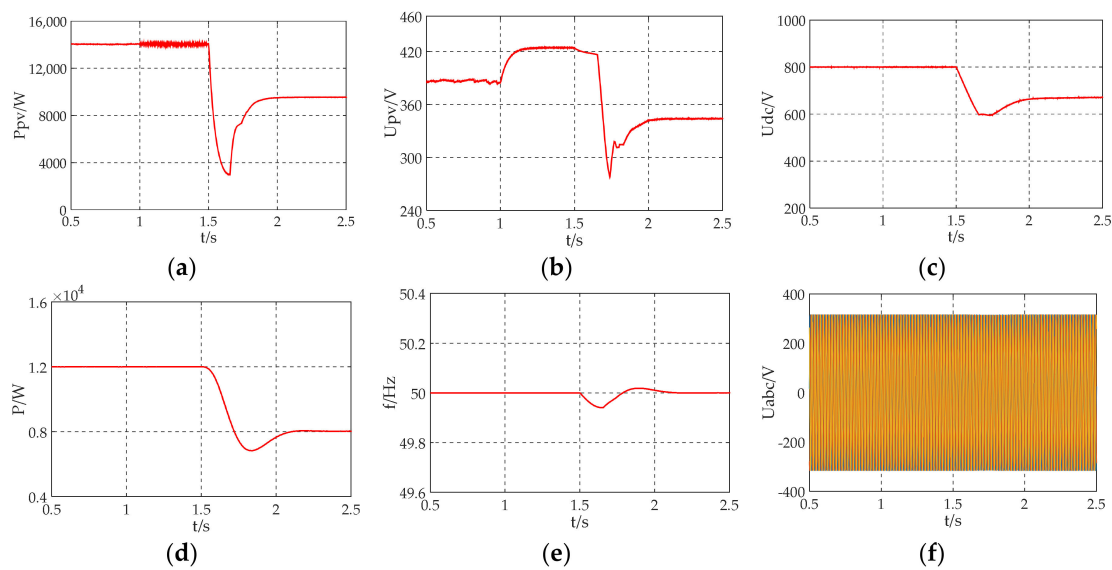


Figure 15. Waveforms in the grid-connected mode when PV maximum output power changes (a) PV output power; (b) PV output voltage; (c) DC bus voltage; (d) Inverter output power; (e) VSG frequency; (f) Inverter output voltage.

Before 1 s, when the light intensity is 1000 W/m^2 , the PV maximum output power is 15 kW, which is more than the dispatching demand 12 kW. Accordingly, from Figure 15a,b,d, the PV managed by adaptive-MPPT alters the working point in the stable voltage range ($U_{pv} > 370 \text{ V}$) to enable inverter power output to meet dispatching power need of 12 kW. At 1 s, the light intensity is amplified to 1200 W/m^2 so that MPP point is (18.2 kW, 380 V). Even if the light intensity strengthens, PV still operates in the stable region ($U_{pv} > 380 \text{ V}$) to send invariant power owing to the constant dispatching power demand. Moreover, since this above regulation ensures supply-demand matching, Figure 15c shows that the DC bus voltage remains at the set value of 800 V. After 1.5 s, the light intensity weakens to 700 W/m^2 , at this moment, PV maximum output power fails to satisfy the dispatching power requirement, i.e., $P_{\max} = 9.5 \text{ kW} < P_{\text{need}} = 12 \text{ kW}$, so it can be seen from Figure 15a,b that PV power transforms into traditional MPPT operation (9.5 kW, 342 V) to lower power shortage. Additionally, improved-VSG control takes effect to stabilize DC bus voltage at 655 V. Similar to the variation of the dispatching power demand in grid-connected mode, in the steady state, the VSG frequency in Figure 15e and inverter output voltage in Figure 15f are identical to the frequency and voltage of the bulk power grid.

To summarize, based on the simulation results and simulation analysis of the Figures 12–15, the effectiveness of the proposed two-stage PV-VSG approach based on adaptive-MPPT has been demonstrated. Whether in off-grid mode or grid-connected mode, no matter when the power demand changes or the light intensity changes, PV power can operate in a stable area to adjust adaptively, and PV-VSG can provide the most effective output power matching under different load/dispatching power requirements, guaranteeing system stability in conditions of insufficient PV power. Accordingly, compared with traditional two-stage PV-VSG equipped with additional energy storage on the DC bus [19–22], the proposed control method reduces the cost of investment and operation on account of not configuring energy storage.

5. Conclusions

In order to address the increasing energy crisis and environmental pollution, photovoltaic power generation is highly regarded because of its sustainable nature, which can develop a circular economy. In terms of PV control, PV systems built on economic benefits mostly work in MPPT mode, which is not in a position to satisfy the operational demands of the future power system owing to the inability to provide inertia and damping support for the grid. VSG technology is emerging as an attractive

solution for the above problem, but traditional PV-VSG ordinarily assembles energy storage devices, which cause many limitations in terms of various costs. Therefore, following consideration of dynamic characteristics of PV output, adaptive-MPPT-based control of an improved two-stage PV-VSG is proposed. The suggested strategy permits PV-VSG to inject power to the loads or grid in light of the power requirements under the circumstances of adequate PV power; in the case of inadequate PV power, the PV system can implement full output due to the conversion of adaptive-MPPT to traditional MPPT, and improved-VSG enhances the stability of PV-VSG. The accuracy of the proposed model has been proven through MATLAB/Simulink. The main contribution of this paper is that a two-stage PV-VSG can be interfaced with loads or the power grid without requiring energy storage allocation. The presented approach can be applied in high-permeability PV regions, future grids with access to a large number of PVs, and in some areas hoping to reduce costs, space occupation, and post-maintenance, and takes on better scalability.

Author Contributions: X.Y. proposed the research direction, adaptive-MPPT method and improved-VSG strategy. J.L. completed the adaptive-MPPT algorithm and improved-VSG control approach. X.Y., J.L., L.W., S.Z., T.L., Z.L. and M.W. performed the verification and analyzed the results. J.L. wrote the paper.

Acknowledgments: This paper was supported by the National Key R&D Program of China (2016YFB0900400); Natural Science Foundation of Hebei Province (E2018502134); State Grid Corporation of Science and Technology Project (PD71-17-008); Liaoning Power Grid Corporation's 2018 Science and Technology Project "Research on the Reactive Power and Voltage Optimization Strategy and Evaluation Index Considering Source and Load Fluctuation Characteristics".

Conflicts of Interest: The authors declare no conflict of interest.

References

1. Yang, X.; Song, Y.; Wang, G.; Wang, W. A comprehensive review on the development of sustainable energy strategy and implementation in China. *IEEE Trans. Sustain. Energy* **2010**, *1*, 57–65. [CrossRef]
2. Cucchiella, F.; D'Adamo, I.; Gastaldi, M. Economic Analysis of a Photovoltaic System: A Resource for Residential Households. *Energies* **2017**, *10*, 814. [CrossRef]
3. Zsiborács, H.; Hegedűsné Baranyai, N.; Vincze, A.; Háber, I.; Pintér, G. Economic and Technical Aspects of Flexible Storage Photovoltaic Systems in Europe. *Energies* **2018**, *11*, 1445. [CrossRef]
4. Liu, J.; Long, Y.; Song, X. A Study on the Conduction Mechanism and Evaluation of the Comprehensive Efficiency of Photovoltaic Power Generation in China. *Energies* **2017**, *10*, 723.
5. Han, P.; Lin, Z.; Wang, L.; Fan, G.; Zhang, X. A Survey on Equivalence Modeling for Large-Scale Photovoltaic Power Plants. *Energies* **2018**, *11*, 1463. [CrossRef]
6. National Development and Reform Commission, Ministry of Finance, National Energy Administration. Notice on Matters Related to Photovoltaic Power Generation in 2018. Available online: http://www.ndrc.gov.cn/gzdt/201806/t20180601_888639.html (accessed on 31 May 2018).
7. Su, M.; Luo, C.; Hou, X.; Yuan, W.; Liu, Z.; Han, H.; Guerrero, J.M. A communication-free decentralized control for grid-connected cascaded PV inverters. *Energies* **2018**, *11*, 1375. [CrossRef]
8. Chen, D.; Jiang, J.; Qiu, Y.; Zhang, J.; Huang, F. Single-stage three-phase current-source photovoltaic grid-connected inverter high voltage transmission ratio. *IEEE Trans. Power Electron.* **2017**, *32*, 7591–7601. [CrossRef]
9. Zhong, Q.C.; Weiss, G. Synchronverters: Inverters that mimic synchronous generators. *IEEE Trans. Ind. Electron.* **2011**, *58*, 1259–1267. [CrossRef]
10. Chen, D.; Xu, Y.; Huang, A.Q. Integration of dc microgrids as virtual synchronous machines into the ac grid. *IEEE Trans. Ind. Electron.* **2017**, *99*, 7455–7466. [CrossRef]
11. Zhong, Q.C. Virtual synchronous machines: A unified interface for grid integration. *IEEE Power Electron. Mag.* **2016**, *3*, 18–27. [CrossRef]
12. National Energy Administration. Guidance on Promoting Smart Grid Development. Available online: http://www.ndrc.gov.cn/gzdt/201507/t20150706_736625.html (accessed on 6 June 2018).
13. Zheng, T.; Chen, L.; Liu, W.; Guo, Y.; Mei, S. Multi-mode operation control for photovoltaic virtual synchronous generator considering the dynamic characteristics of primary source. *Proc. CSEE* **2017**, *37*, 454–464. (In Chinese)
14. Shintai, T.; Miura, Y.; Ise, T. Oscillation damping of a distributed generator using a virtual synchronous generator. *IEEE Trans. Power Del.* **2014**, *29*, 668–676. [CrossRef]

15. Shi, K.; Zhou, G.; Xu, P.; Ye, H.; Tan, F. The integrated switching control strategy for grid-connected and islanding operation of micro-grid inverters based on a virtual synchronous generator. *Energies* **2018**, *11*, 1544. [[CrossRef](#)]
16. Yao, G.; Lu, Z.; Wang, Y.; Benbouzid, M.; Moreau, L. A virtual synchronous generator based hierarchical control scheme of distributed generation systems. *Energies* **2017**, *10*, 2049. [[CrossRef](#)]
17. Zheng, T.; Chen, L.; Guo, Y.; Mei, S. Comprehensive control strategy of virtual synchronous generator under unbalanced voltage conditions. *IET Gener. Transm. Dis.* **2018**, *12*, 1621–1630. [[CrossRef](#)]
18. Wu, H.; Ruan, X.; Yang, D.; Chen, X.; Zhao, W.; Lv, Z.; Zhong, Q.C. Small-signal modeling and parameters design for virtual synchronous generators. *IEEE Trans. Ind. Electron.* **2016**, *63*, 4292–4303. [[CrossRef](#)]
19. Yan, X.; Zhang, X.; Zhang, B.; Ma, Y.; Wu, M. Research on distributed PV storage virtual synchronous generator system and its static frequency characteristic analysis. *Appl. Sci.* **2018**, *8*, 532. [[CrossRef](#)]
20. Mao, M.; Qian, C.; Ding, Y. Decentralized coordination power control for islanding microgrid based on PV/BES-VSG. *CPSS TPEA* **2018**, *3*, 14–24. [[CrossRef](#)]
21. Liu, J.; Miura, Y.; Ise, T. Comparison of dynamic characteristics between virtual synchronous generator and droop control in inverter-based distributed generators. *IEEE Trans. Power Electron.* **2016**, *31*, 3600–3611. [[CrossRef](#)]
22. Gao, B.; Xia, C.; Chen, N.; Cheema, K.; Yang, L.; Li, C. Virtual synchronous generator based auxiliary damping control design for the power system with renewable generation. *Energies* **2017**, *10*, 1146. [[CrossRef](#)]
23. Guo, Y.; Chen, L.; Li, K.; Zheng, T.; Mei, S. A novel control strategy for stand-alone photovoltaic system based on virtual synchronous generator. In Proceedings of the 2016 IEEE Power and Energy Society General Meeting (PESGM), Boston, MA, USA, 17–21 July 2016; pp. 1–5.
24. Mei, S.; Zheng, T.; Chen, L.; Li, C.; Si, Y.; Guo, Y. A comprehensive consensus-based distributed control strategy for grid-connected PV-VSG. In Proceedings of the 2016 35th Chinese Control Conference (CCC), Chengdu, China, 27–29 July 2016; pp. 10029–10034.
25. Fu, Y.; Wang, Y.; Zhang, X. Integrated wind turbine controller with virtual inertia and primary frequency responses for grid dynamic frequency support. *IET Renew. Power Gen.* **2017**, *11*, 1129–1137. [[CrossRef](#)]
26. Zhang, Z.S.; Sun, Y.Z.; Lin, J.; Li, G.J. Coordinated frequency regulation by doubly fed induction generator-based wind power plants. *IET Renew. Power Gen.* **2012**, *6*, 38–47. [[CrossRef](#)]
27. Wang, Y.; Meng, J.; Zhang, X.; Xu, L. Control of PMSG-based wind turbines for system inertial response and power oscillation damping. *IEEE Trans. Sustain. Energy* **2015**, *6*, 565–574. [[CrossRef](#)]
28. Hua, T.; Yan, X.; Fan, W. Research on power point tracking algorithm considered spinning reserve capacity in grid-connected photovoltaic system based on VSG control strategy. In Proceedings of the 2017 IEEE 3rd International Future Energy Electronics Conference and ECCE Asia (IFEEC 2017—ECCE Asia), Kaohsiung, Taiwan, 3–7 June 2017; pp. 2059–2063.
29. Tang, L.; Xu, W.; Mu, C. Analysis for step-size optimisation on MPPT algorithm for photovoltaic systems. *IET Power Electron.* **2017**, *10*, 1647–1654. [[CrossRef](#)]
30. Killi, M.; Samanta, S. Modified perturb and observe MPPT algorithm for drift avoidance in photovoltaic systems. *IEEE Trans. Ind. Electron.* **2015**, *62*, 5549–5559. [[CrossRef](#)]
31. Zhang, B.; Yan, X.; Li, D.; Zhang, X.; Han, J.; Xiao, X. Stable operation and small-signal analysis of multiple parallel DG inverters based on a virtual synchronous generator scheme. *Energies* **2018**, *11*, 203. [[CrossRef](#)]
32. D’Arco, S.; Suul, J.A. Equivalence of virtual synchronous machines and frequency-droops for converter-based microgrids. *IEEE Trans. Smart Grid* **2014**, *5*, 394–395. [[CrossRef](#)]

